34th Annual International Conference of the IEEE EMBS
San Diego, California USA, 28 August - 1 September, 2012

Implementation and Evaluation of Hyperelastic Model for Surgical Simulator and Navigation

Masato Ogata[1], Yasunori Dohi[2], Takahiro Yamada[3], and Yoshinobu Kubota[4]

***Abstract*— We developed a practical laparoscopic surgical simulator using co-rotated FEM in a linear scheme. This was somewhat of a compromise due to a strong constraint on real-time processing. The spread of surgical simulators and medical simulations for clinical medicine in the near future will impose important demands that cannot be met with this linear scheme. For example, subtle force sensing by forceps used for peeling connective tissues and moving blood vessels is very important for a preoperative surgical simulator, as is precisely predicting the deformation of organs with patient posture during surgery for torocar simulation and surgical navigation. We evaluated several models such as co-rotated FEM, nonlinear FEM, and the hyperelastic model for these advanced real-time medical applications. As a result, we confirmed that the hyperelastic model is the most suitable for the anticipated surgical simulator, and that the co-rotated FEM and nonlinear FEM score almost the same in both processing time and accuracy. In addition, implementation of the hyperelastic model in real time seems possible with current off-the-shelf PCs.**

I. Introduction

We developed a laparoscopic surgical simulator using improved co-rotated FEM based on a linear FEM scheme[7][8] that compensates for stress caused by rigid rotation. This is a compromise based on time-critical constraint. In response to the rapidly expanding use of surgical simulation and surgical navigation in clinical applications in the near future, there will be important functions that cannot be implemented with the linear scheme. For example, deformation of the organs due to changes in the patient posture and a specific feeling of subtle force over the region for removing connective tissue and treatment of arteries. For these reasons, it is important to analyze and evaluate the characteristics of the models with real-time processing. This report presents an evaluation of the characteristics of each model (rotation correction, geometrical nonlinear, Mooney-Rivlin hyperelastic model) with numerical experiments. For the experiment, we reorganized and implemented a geometrical nonlinear FEM and a co-rotated FEM that assumes material linearity based on the previous work, and a newly implemented hyperelastic model that has material nonlinearity.

[1]M. Ogata with the R & D Division, Mitsubishi Precision Co.,Ltd., 345 Kamimachiya, Kamakura, Japan, and also belongs to the Graduate School of Medicine, Yokohama City University ogatamt at yokohama-cu.ac.jp

[2]Y. Dohi is with the Graduate School of Electrical Engineering, Yokohama National University, 79-5 Tokiwadai Hodogaya Yokohama Japan dohi at ynu.ac.jp

[3]T. Yamada is with the Graduate School of Environment and Information Sciences, Yokohama National University, 79-7 Tokiwadai Hodogaya Yokohama Japan tyamada at ynu.ac.jp

[4]Y. Kubota is with the Graduate School of Medicine, Yokohama City University, 3-9 Fukuura Kanazawa-ku Yokohama Japan kubotayo at med.yokohama-cu.ac.jp

Unfortunately, there are no scientific data in particular on the mechanical properties during surgery that are expected to be used for validating many surgical simulators and navigation systems. This report is an evaluation of the first step in the series envisioned in the study regarding real-time models from the engineering point of view. The final evaluation will be performed taking into account the results of in vivo experiments with laboratory animals using a measuring device (currently under development) that can gather images and forces at the same time.

Section II describes the weak form of the nearly-incompressible Mooney-Rivlin model based on the principle of stationary potential energy. We then explain the verification of the implemented model using nonlinear FEM software ADINA in Section III. In Section IV, we evaluate the behavior and characteristics of the implemented models. Finally, we state our conclusions in Section V.

II. Nearly-Incompressible hyper elastic model with Perturbed method

The Mooney-Rivlin model is used to represent the elastic potential energy function of hyperelastic material.

Let W^M be the elastic energy density function of the Mooney-Rivlin model,

$$W^M = c_1(\tilde{I_C} - 3) + c_2(\tilde{I\!I_C} - 3) \tag{1}$$
$$\tilde{I_C} \equiv I_C I\!I\!I_C^{-\frac{1}{3}}, \tilde{I\!I}_C \equiv I\!I_C I\!I\!I_C^{-\frac{2}{3}} \quad ,$$

where $I_C, I\!I_C$ and $I\!I\!I_C$ are the first, second, and third invariants of right Cauchy-Green deformation tensor $\boldsymbol{C}$. Adding an energy term due to volumetric change in the elastic energy density function and a constraining term to inhibit volumetric change, then integrating this over analytical volume area Ω and surface S yields the potential energy $\tilde{\Phi}_{ptb}$ of the *perturbed Lagrange-multiplier method* [1][2][4][5].

$$\tilde{\Phi}_{ptb} = \int W^M d\Omega + \int \lambda \underbrace{(J-1)}_{W^V} d\Omega$$
$$-\frac{1}{2}\int \frac{1}{\alpha}\lambda^2 d\Omega + \underbrace{\int R dS + \int Q d\Omega}_{\Phi_{ext}} \quad , \tag{2}$$

where, λ indicates the Lagrange multiplier, J is volume, α corresponds to the bulk modulus, $\boldsymbol{R}$ is the surface force, and $\boldsymbol{Q}$ is the body force. We assume no total energy change due to external force in the following discussion.

By calculating the first variant $\delta_{\boldsymbol{u}}\tilde{\Phi}_{ptb}$ and $\delta_{\boldsymbol{\lambda}}\tilde{\Phi}_{ptb}$ corresponding to displacement $\boldsymbol{u}$ and Lagrange multiplier $\boldsymbol{\lambda}$, we obtain the following equilibrium conditions. To solve the above stationary energy problem is equivalent to solving the

978-1-4577-1787-1/12/$26.00 ©2012 IEEE

following equations.

$$\int_\Omega \left(\frac{\partial W^M}{\partial C_{ij}} + \lambda \frac{\partial W^V}{\partial C_{ij}} \right) \delta C_{ij} d\Omega$$
$$= \int_{\partial\Omega} \boldsymbol{t} \cdot \delta \boldsymbol{u} dS + \int_\Omega \rho_0 \boldsymbol{g} \cdot \delta \boldsymbol{u} d\Omega \quad (3)$$

$$\int \left[(W^V - \frac{\lambda}{\alpha}) \delta\lambda \right] d\Omega = 0 \quad (4)$$

We approximated the above equations using the finite element method and implemented a nearly-incompressible hyperelastic model. We first implemented the model based on the *projective method* [6], but we initially misunderstood the reason for the instability of the calculations inherent in the model so we also implemented the *perturbs Lagrange method*. Although the energy functions differ[1], we found that the derived weak-form Eqs.(3) and (4) are identical to that of the *projective method* so the two methods seem equivalent. In addition, instability in numerical calculations is a common problem inherent in the concavity of the energy functions[3].

III. Verification of the Implemented Model

It is necessary to create our own code for real-time implementation of a hyperelastic model. However, the nonlinear finite-element method, in particular on tensor calculations in hyperelastic material, is so complicated that it becomes easy to make errors. To verify the implemented code, we used nonlinear finite-element method software called ADINA to verify the results of two different data density cases.

A. Conditions for verificationF finite element approximation,material properties,constraints

For surgical simulator, using a tetrahedral finite element is suitable for geometrical shape approximation. We used 1101 elements and 401 nodes of the tetrahedral artery model for verification. As the interpolation function, we used a four point first-order approximation for the displacement and one point for pressure as seen in TABLE I. Unfortunately, this does not satisfy the *inf-sup* criteria of *Ladyszhenskaya-Babuska-Brezzi-KikuchiiLBBK)* [3]. For a surgical simulator, however, it is reasonable to adopt that shape function because (1) the criteria indirectly show that a situation in which the equations are greater than the unknown has never happened in a surgical simulator, and (2) the process is highly time-critical.

We used TABLE II for material properties. To adjust the runtime conditions, we used 4α, as explained later, in the simulator as ADINA's bulk modulus κ. We performed the large deformation indicated in Fig. 1 using the above runtime conditions. As seen in the figure, the positions of the top nodes are fixed, the x position of the middle nodes are moved 50% of the width (free for y and z directions), and the position of the bottom nodes are moved 30% of the height in the z direction (free for x and y directions).

B. Verification with ADINA

TABLE III compares the deformation between ADINA and the implemented simulator for a nearly-incompressible hyperelastic model. Subtable (a) compares the displacement,

[1] $\bar{\Phi}_{prj} = \int W^M d\Omega + \frac{\kappa}{2} \int Prj(W^V)^2 \lambda d\Omega + \Phi_{ext}, \quad Prj(\kappa W^V) = \lambda$

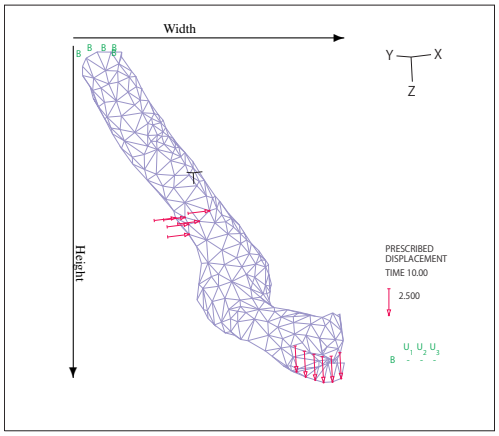

Fig. 1. Position constraints for verification with ADINA. The position of the top nodes are fixed, the x position of the middle nodes are moved 50% of the width(free for y, and z directions), and the position of the lowest nodes are moved 30% of the height in the z direction (free for x and y directions).

TABLE I

FEM APPROXIMATION FOR EACH MODEL

Model	Displacement. Order	Pressure Order	Gauss Integration Gauss Points
Linear FEM	First order 4 points	-	-
Co-Rotated FEM	First order 4 points	-	-
Geometrical NLFEM	First order 4 points	-	4 points
Hyperelastic iMooney)	First order 4 points	1point	4points

and subtable (b) indicates the relative error on each node and the average relative error for all nodes. The average error is less than 2% for 5.1kg/m3 density and is 1% for the 510kg/m3 case. From this result, we conclude that the implementation is correct. In addition, the difference in processing between geometrical nonlinear FEM model and the Mooney-Rivlin model is seen only in the calculating on the stress tensor, so we conclude that the geometrical nonlinear FEM is also implemented correctly.

Although the commonly accepted solvable conditions for simultaneous equations, i.e. a positive definition of the stiffness matrix for the conjugate gradient method, are not guaranteed for the nearly- incompressible hyperelastic mode, we can get the correct result, as mentioned in Suzukifs paper [9].

TABLE II

MATERIAL PROPERTIES FOR EXPERIMENTS: FOR MOONEY-RIVLIN MODEL, EQUIVALENT $c_1 + c_2$ AND α ARE CONVERTED FROM YOUNG'S MODULUS AND POISSON RATIO AND THEN SEPARATED INTO c_1 AND c_2.

Finite Element Model	Linear material		Nonlinear material		
	Young's Modulus	Poisson	c_1	c_2	α
Linear	1MPa	0.49	-	-	-
Co-Rotated	1MPa	0.49	-	-	-
Geometrical Nonlinear	1MPa	0.49	-	-	-
Mooney-Rivlin	-	-	1.343 $\times 10^5$	0.335 $\times 10^5$	4.167 $\times 10^6$

TABLE III

VERIFICATION FOR IMPLEMENTED NEARLY-INCOMPRESSIBLE HYPERELASTIC MODEL WITH ADINA

(a) Comparison of nodal displacement

Node No.	Density$\rho = 510\mathrm{kg/m^3}$						Density$\rho = 5.1\mathrm{kg/m^3}$					
	Displacement by ADINA			Displacement by implemented Simulator			Displacement by ADINA			Displacement by implemented Simulator		
	x		z	x	y	z	x	y	z	x	y	z
1	1.2374	0.6295	0.6913	1.2326	0.6236	0.6867	1.2489	0.6125	0.6257	1.2363	0.6196	0.6118
45	2.5000	1.9100	0.7110	2.5000	1.9016	0.6988	2.5000	1.8887	0.6046	2.5000	1.8918	0.5746
46	2.2106	1.6410	1.0841	2.1936	1.6294	1.0799	2.2237	1.6186	0.9724	2.1900	1.6209	0.9647
47	2.2708	1.7039	0.9784	2.2591	1.6975	0.9715	2.2801	1.6793	0.8700	2.2584	1.6920	0.8586
48	2.0747	1.4752	0.9899	2.0601	1.4672	0.9818	2.0895	1.4520	0.8819	2.0591	1.4585	0.8661
100	1.7181	1.1306	0.6531	1.7080	1.1159	0.6441	1.7333	1.1211	0.5446	1.7094	1.1032	0.5273
150	0.5841	0.1487	0.3183	0.5790	0.1414	0.3126	0.5814	0.1433	0.2874	0.5733	0.1430	0.2766
200	1.6391	2.6001	1.6142	1.6294	2.6014	1.6012	1.6217	2.5603	1.5319	1.5849	2.5805	1.5075
250	1.6399	2.3910	1.9311	1.6290	2.3737	1.9227	1.6177	2.3610	1.8626	1.5700	2.3364	1.8471
300	1.5931	2.6082	1.6256	1.6113	2.6067	1.6131	1.5534	2.5735	1.5481	1.5810	2.5700	1.5162
350	1.0939	2.3761	2.5134	1.0866	2.3467	2.5102	1.0533	2.3700	2.4751	1.0215	2.3106	2.4592
400	1.1094	2.1033	2.8546	1.0872	2.0550	2.8568	1.0749	2.1081	2.8108	1.0053	1.9962	2.8048

(b) Nodal displacement error

Node	Density$\rho = 510\mathrm{kg/m^3}$ $\lvert Adina - Sim\rvert / \lvert Adina\rvert * 100$			Density $\rho = 5.1\mathrm{kg/m^3}$ $\lvert Adina - Sim\rvert / \lvert Adina\rvert * 100$		
	(%)	(%)	(%)	(%)	(%)	(%)
1	0.3927	0.9586	0.6622	1.0112	1.1539	2.2242
45	0.0000	0.4405	1.7143	0.0000	0.1645	4.9638
46	0.7673	0.7083	0.3872	1.5144	0.1412	0.7901
47	0.5145	0.3791	0.6995	0.9518	0.7548	1.3130
48	0.7030	0.5413	0.8179	1.4561	0.4530	1.7907
100	0.5847	1.3113	1.3790	1.3757	1.5995	3.1751
150	0.8735	4.8830	1.7888	1.3924	0.2184	3.7774
200	0.5880	0.0444	0.8029	2.2654	0.7891	1.5910
250	0.6692	0.7245	0.4335	2.9452	1.0442	0.8322
300	1.1405	0.0600	0.7668	1.7802	0.1359	2.0592
350	0.6682	1.2292	0.1301	3.0214	2.5106	0.6418
400	2.0006	2.2992	0.0761	6.4780	5.3072	0.2157
	Average displacement error 0.89 %			Average Displacement error 1.72%		

IV. MODEL EVALUATIONS

A. Artery model

We evaluate the behavior of each mathematical model using artery data from near the kidney to create conditions similar to the surgical simulator with two different densites. It is difficult to adjust the material properties of the hyperelastic model, which has nonlinear material properties compared to the other models, which all have linear material properties. We therefore use the following conversion relating Poisson ratio and Young's modulus to c_1 and c_2 of the Mooney-Rivlin's parameters.

$$c_1 + c_2 = \frac{E}{4(1+\nu)} \;\; ; \;\; \alpha = \frac{E}{12(1-2\nu)}$$

The relation between the bulk modulus κ of ADINA and α of Eq.(4) thus becomes $\kappa = 4\alpha$. We conducted an evaluation with a first-order four-nodal interpolation as the shape function and a four points Gauss integration for the nonlinear FEM as indicated in TABLE I using the material properties in TABLE II for the two different density cases. The resultant deformations are presented in Fig. 2. A nodal displacement comparison between geometrical nonlinear FEM and co-rotated FEM, and between geometrical nonlinear FEM and linear FEM is given in TABLE IV. The average displacement error is 6.1% and the maximum error is 43% in the co-rotated FEM case. The average displacement error is 36% and the maximum error is 58% in the linear FEM case.

B. Experiment results

Experiment with laboratory animals are necessary before the final decision, but we currently have the following results.

(a) The Mooney-Rivlin model is the best model for simulator as expected. Even for self-weight deformation, it produces behavior similar to the real case. The image appears in Figs. 2(a)(b).

(b) The volumetric increase is noticeable in linear FEM for large deformations as is well known. The calculation cost is low but it cannot be applied to a simulator for trainning in artery treatment. The image appears in Fig. 2(c).

TABLE IV

COMPARISON OF DISPLACEMENT ERROR IN GEONLFEM AND CORFEM, GEONLFEM AND LINEAR FEM: DENSITY IS $\rho = 5.1 \times 10^3 \mathrm{kg/m^3}$

Node	$\lvert GNL - COR\rvert / \lvert NONL\rvert$%			$\lvert GNL - LN\rvert / \lvert NONL\rvert$%		
	(%)	(%)	(%)	(%)	(%)	(%)
1	0.5112	2.7307	18.1435	9.1842	37.1625	54.3600
45	0.0000	1.4042	11.5888	0.0000	49.1189	58.9639
46	0.3273	2.1791	7.7978	3.9853	40.3690	53.0914
47	0.7620	0.5687	9.1888	1.4450	42.3155	55.1929
48	1.0265	1.1255	10.0142	1.5526	40.8137	54.3329
100	0.5890	0.5687	10.7654	4.8364	47.8368	53.3939
150	1.8382	27.1952	43.2574	1.8382	27.1952	43.2574
200	1.0926	0.2909	3.1229	35.3661	56.0217	31.2568
250	2.8405	0.2272	2.1223	37.5813	58.4354	17.4508
300	0.8777	0.7175	2.1331	31.6699	59.1114	13.7821
350	3.7965	9.1566	12.4086	53.9827	66.8742	19.3299
400	11.3192	7.7658	10.1314	58.0800	64.4939	0.2555
	Average displacement error 6.1%			Average displacement error 35.7%		

TABLE V

COMPARISON OF MODEL PROCESSING TIMES

Model	Generation of stiffness matrix	Solving Simultaneous EQ
Linear FEM	0.09	4.2
Co-Rotated FEM	1	4.2
Nonlinear FEM	1.3	4.2
Mooney Rivlin	10.1	19.8

Indicated figures are ratios to the time of stiffness matrix generation in co-rotated FEM.

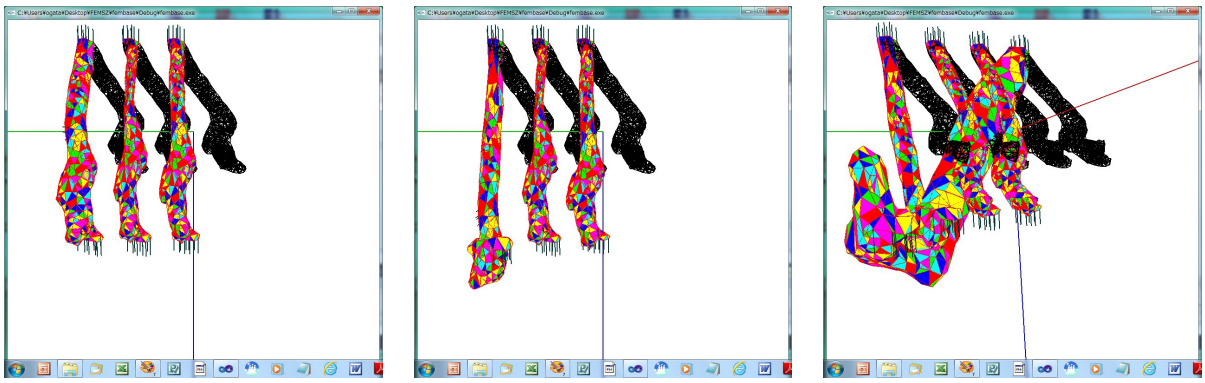

(a) Deformations of Mooney-Rivlin, GNLFEM, and CORFEM models are shown from left to right. Density is $5.1 \times 10^3 \mathrm{kg/m}^3$. The black line drawings are the images from before deformation.

(b) Deformations of Mooney-Rivlin, GNLFEM and CORFEM models are shown from left to right. Density is $510 \times 10^3 \mathrm{kg/m}^3$. The black line drawings are the images from before deformation.

(c) Deformation of Mooney-Rivlin, GNLFEM, CORFEM and Linear FEM models are shown from left to right. Density is $510 \times 10^3 \mathrm{kg/m}^3$. Volume increase of Linear FEM is noticeable in large deformation.

Fig. 2. Simulation results of each model using artery data: Young's modulus is 1Mpa, Poisson ratio is 0.49 for linear material; The corresponding material properties are $c_1 + c_2 = 1.67853 \times 10^5$,$c_2 : c_1 = 1 : 4$,$\alpha = 4.166667 \times 10^6$ for the Mooney -Rivlin model. The boundary is given in Fig. 1. The solver is the conjugate gradient method.

(c) The difference between the deformations of co-rotated FEM and geometrical nonlinear FEM is not noticeable at life-scale sizes. To use co-rotated FEM for a surgical simulator seems appropriate given these results. As for surgical navigation, which requires precise positioning, co-rotated FEM has an average 7% error as seen in TABLE IV, so it could not be applied for that purpose.

C. Discussions of implementation of MR. model in real-time

The Mooney-Rivlin model uses the Newton-Raphson method to obtain the nodal displacement. For implementing the Mooney-Rivlin in a surgical simulator, i.e., in real-time, we suppose that to correspond the simulator's one iteration to Newton Raphson's one iteration is reasonable. Because the deformation is very small over that time span. Our experience of implementing the conjugate gradient method in a GPU, i.e., more than twenty times faster than the speed of a CPU, suggests that it is possible to implement a nearly-incompressible hyperelastic model in real time.

V. Conclusions

We developed a practical laparoscopic surgical simulator using co-rotated FEM in a linear scheme. It was somewhat of a compromise due to strong constraints on real-time processing. The spread of surgical simulators and medical simulations for clinical medicine in the near future will place strong demands which cannot be met with a linear scheme. For example, subtle force sensing by forceps for peeling connective tissues and moving blood vessels is very important for a preoperative surgical simulator, as is precisely predicting the deformation of organs with patient posture during surgery for torocar simulation and surgical navigation. We implemented and evaluated several models, including the co-rotated FEM, nonlinear FEM, and hyperelastic models, for these advanced real-time medical applications. As a result, we confirmed that the hyperelastic model is the most suitable for a surgical simulator as anticipated and that the co-rotated FEM and geometrical nonlinear FEM are almost the same in both processing time and positioning accuracy. In addition, it seems possible to implement the hyperelastic model in real time with current off-the-shelf PCs.

Acknowledgment

The authors thank Dr. Kazuhide Makiyama of the Graduate School of Medicine at Yokohama City University for collaboration on this research. Part of this research was supported by Grants-in-Aid for Scientific Research, MEXT(Nos. 23390383 and 23659762).

References

[1] T.Y.P Changl , F. Saleeb and G. Li, Large strain analysis of rubber-like materials based on a perturbed Lagrangian variational principle, Computational Mechanics Vol.8,No.8 pp.221-233, 1991

[2] S.N. Atluri and Reissner, On the formulation of variational theorems involving volume constraints,Computational Mechanics Vol.5, No.8 pp.337-344,1989

[3] F. Brezzi, On Existence, uniqueness and approximation of saddle-point problems arising from Lagrangian Multipliers, RAIRO, Vol8, pp.129-151,1974

[4] T. Sussman, K.J. Bathe, A finite element formulation for nonlinear incompressible elastic and inelastic analysis, Computers and Structures Vol. 26, pp.357-409,1987

[5] G.A. Holzapfel, Nonlinear solid mechnics, pp.406-407, John Wiley & Sons,Ltd., 2000

[6] K. Watanabe, Lecture note in special lecture for nonlinear FEM, Tokyo University, 2010

[7] Y. Dohi, M. Ogata, A basic study for surgical simulator, technical report of Mitsubishi Precision Co.,Ltd., Vol. 1, 2010

[8] M. Ogata, M.Nagasaka, T. Imuiya, K. Makiyama, Y. Kubota, A Development of Surgical Simulator for Training of Operative Skills using Patient-Specific Data, Studies in Health Technology and Informatics, Vol. 163, pp.415-421, IOCS Press, 2011

[9] A. Suzuki, M. Tabata, Convergence of conjugate gradient method for symmetric indefinite matrix, bulletin of Research Institute for Mathematical Sciences Kyoto University , Vol 1265, pp 39-44, 2002